RSC Advances

Journal Name

ARTICLE

Modified Bridgman growth and characterization of a novel mid-infrared transparent optical crystal: LiGa$_3$Te$_5$

Shanpeng Wang, [a] Guandong Liu, [a] Qiong Shi, [a] Xiang Zhang, [a] Xixia Zhang, [a] Chunlong Li, [a] Zeliang Gao, [a] Chunming Dong, [a] Qingming Lu, [b] Xutang Tao [*a]

A large single LiGa$_3$Te$_5$ (LGT) crystal was grown with sizes up to Ø16 mm × 50 mm for the first time using a modified vertical Bridgman-Stockbarger method. LGT crystallizes in the non-centrosymmetric system, space group R32, with a = b = 14.343(7) Å, c = 17.617 Å, Z = 12, and V = 3139 Å3. A detailed description of the polyhedral connections in the LGT structure is presented. The X-ray rocking curve, specific heat and thermal conductivity are also investigated. The room-temperature transmission of the as-grown LGT without any coating is above the 40% level from 3.5 to 18 µm. The cut-off edges at short and long wavelength are 0.9 and 25 µm, respectively. Owing to its wide transparency range, LGT is a promising candidate for MIR and far-infrared NLO applications, and even for THz transmission and generation.

Journal Name

ARTICLE

Introduction

Widely tunable coherent mid-infrared (MIR) laser sources, especially in band II (3-5μm) and band III (8-12μm) of the three transparent atmospheric windows, are of great importance for military and civilian applications, such as directional infrared countermeasures (DIRCM), infrared guidance, sensing for organic and inorganic molecules, and medical applications. [1-4] Although, many direct ways can realize MIR lasers, such as semiconductor lasers,[5, 6] Tm and Ho-doping lasers,[7] Er^{3+}-lasers, tunable Cr^{2+}-lasers,[8-10] and quantum cascade laser (QCL),[11, 12] etc. The applications with these aforementioned lasers are restricted due to few suitable laser transitions with long living upper state and the exotic pump lasers requirement. Therefore, frequency conversion by nonlinear optical (NLO) crystals is recognized as a powerful and viable way of producing tunable coherent mid-infrared lasers. Oxide NLO crystals can be pumped by widely-spread high-power diode-pumped lasers to produce parametric generation. However, the spectral coverage beyond 5 μm is dramatically affected by the onset of multi-phonon mid-IR absorption.[13] Only a few of the available nonlinear crystals are suitable for generation of tunable coherent radiation in the mid-infrared range of 3~20 μm. There are two types of important chalcopyrite NLO crystals, including $A^IB^{III}C^{VI}_2$ (A = Ag; B = Ga, In; C = S, Se, Te) and $A^{II}B^{IV}C^V_2$ (A = Zn, Cd; B = Si, Ge; C = P, As).[14] The silver selenogallate (AgGaSe$_2$) and most developed chalcopyrite zinc germanium phosphide (ZnGeP$_2$, ZGP) crystals can generate mid-IR radiation up to ~10 μm based on OPOs, but it must be pumped above 1 μm to avoid two-photon and residual absorption.[15-21] While silver thiogallate (AgGaS$_2$) can be phase matched for pumping near 1 μm, it has relatively low nonlinearity and poor thermal conductivity.[22, 23] The lithium-containing chalcogenide compounds $Li^IB^{III}C^{VI}_2$ (B = Ga, In; C = S, Se, Te) crystallize in a β-NaFeO$_2$ orthorhombic structure (space group *Pna2$_1$*, point group *mm2*). The lighter Li^+ ions in the structure enlarge the band gap of these compounds and further lead to a high laser induced damage threshold. Therefore, they are considered to be promising materials for NLO applications in the MIR, due to their unique optical properties.[24-26] In general, the infrared cut-off edges of $Li^IB^{III}C^{VI}_2$ crystals depend on Li-C vibrations and shift to longer wavelength in the S, Se, and Te series. Different from other $Li^IB^{III}C^{VI}_2$ compounds, LGT crystallizes in a non-centrosymmetric space group, *R*32.[27]

The LiGe$_3$Te$_5$ compound was first reported by L. Kienle et al. Its structure has been determined at 293 K.[27] Later in 2000, H. J. Deiseroth et al. prepared LGT by solid-state reactions and got the small crystal suitable for data collection.[28] Until now,

large LGT crystals for the measurements of physical properties have not been reported in the literatures.

In this paper, we report on a two-step process of synthesis and modified Bridgman growth of LGT. For the first time, to the best of our knowledge, a large-sized bulk LGT with a diameter of 16 mm and length of 50 mm has been obtained. The LGT structure was re-determined by single crystal X-ray diffraction (XRD) and the detailed connections of the polyhedra are discussed. The results of characterization by XRD, high resolution XRD, and measurements of micro-hardness, density, thermal properties and optical properties are presented. The cut-off edge of LGT at long wavelengths is about 25 μm. Therefore, it is a promising candidate for MIR and far-infrared NLO applications, and even for THz transmission and generation.

Experimental section

Polycrystalline synthesis and crystal growth of LGT

Polycrystalline LGT was synthesized from high purity elemental Li (3N), Ga (5N) and Te (5N) by a two-step method.[29] Binary Ga$_2$Te$_3$ was firstly synthesized by the traditional single-temperature-zone method. Elemental Ga and Te in a stoichiometric molar ratio of 2:3 were loaded into a quartz ampoule which was evacuated to 1.0×10^{-3} Pa and then sealed off. The synthesis furnace was single-temperature-zone coil furnace, which was controlled by an FP23 temperature controller (SHIMANDEN). After slowly heating to 850 °C and maintaining this temperature for 20 h, the samples were cooled down to room temperature at a rate of 50 °C/h. High purity single phase Ga$_2$Te$_3$ (confirmed by XRD) was obtained. Secondly, LGT was synthesized from Li, Ga$_2$Te$_3$ and Te. They were weighed in proportion to the stoichiometry of LiGa$_3$Te$_5$ with excess of 0.2% Li and 0.5% Te and loaded into a graphite crucible. All operations were carried out in a glove box filled with Ar gas in view of the chemical activity of Li and Ga. The crucible was sealed in a carbon-coated quartz ampoule at 1.0×10^{-3} Pa, and then placed in the homogeneous temperature zone of the furnace. It was slowly heated to 900 °C over 50 h. After soaking for 30 h to insure complete reaction and homogeneity of the melt, the furnace was cooled down to room temperature at a rate of 50 °C/h.

LGT crystals were grown by the modified Bridgman technique through spontaneous nucleation in a three-zone vertical furnace. Fig. 1 shows the schematic diagram of the three-zone vertical Bridgman furnace and the temperature distribution. The furnace with the total height of 800 mm was divided into hot zone (Ⅰ) and cold zone (Ⅲ) by an adiabatic baffle. The two zones were independently controlled by two FP23 temperature controllers. In this way a gradient zone (Ⅱ)

was obtained, and the desired temperature gradient could be realized by carefully adjusting the position of the baffle in the furnace and the temperatures of the hot and cold zones.
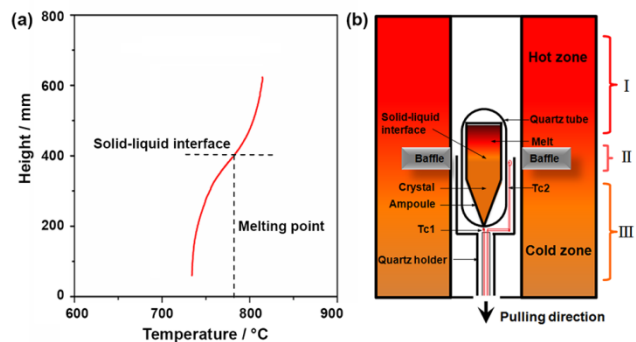
Fig. 1 (a) The axial temperature distribution of the furnace and (b) schematic diagram of three-zone vertical Bridgman furnace. Note that the solid-liquid interface in the ampoule is located nearby the melting point(785±5 °C) of LGT in the gradient zone (II).

The graphite ampoule charged with polycrystalline LGT was put in a quartz tube. The quartz tube was continuously evacuated while being heated for 2 h and then was sealed under the vacuum of 3×10^{-3} Pa. Before crystal growth commenced, the ampoule was placed in the upper region of the furnace. The upper and lower regions of the furnace were heated slowly to 800 °C and 720 °C, respectively, and then soaked for 30 h to insure that the polycrystalline LGT was fully melted and completely homogeneous. The schematic axial temperature distribution of the furnace is shown in Fig. 1(a). The solid-liquid interface in the ampoule is located nearby the melting point (785±5 °C) of LGT. The temperature gradient nearby the solid-liquid interface in the gradient region was 10-15 °C/cm. There are three important modifications to the traditional Bridgman method: (1) The rotation motor can rotate the crucible at an accelerated speed one way and then the other, repeating the cycle periodically, making the LGT melt more homogeneous. (2) Two thermocouples (Tc1 and Tc2) were placed near the cone tip of the crucible and the LGT melt, which was shown in Fig. 1(b). Therefore, the melting state of the polycrystalline LGT and its nucleation could be monitored in-situ during crystal growth. (3) There is growth acceleration at the solid-liquid interface owing to the release of the latent heat of crystallization. As a result, the growth interface is not stable, which is not favourable for the growth of a high quality crystal. Therefore, we optimized the growth process by slowly heating the upper region of the furnace from 800 to 810 °C during the whole crystal growth process in order to prevent growth acceleration. The initial nucleation started from the cone-shaped tip at the bottom of the crucible as it passed through the solid-liquid interface at the LGT melting point. A continuous growth process was maintained by pulling the ampoule down at a rate of 0.5-2 mm/h. The crystal growth interface is located near the solid-liquid interface at the melting point of LGT, as was shown in Fig. 1(b). In order to obtain a high quality crystal, it was very important that the translational

speed of the ampoule coincide with that of the crystal growth. The speed of crystal growth was determined by the intrinsic thermal properties of the melt and the crystal, and also by the temperature gradient at the solid-liquid interface. Therefore, a considerable amount of experimentation was carried out to optimize for suitable temperature gradient and growth parameters. The crystal growth finished when the crucible completely passed through the growth interface into the cold zone. The furnace temperature was then kept constant for 200 h to anneal the crystal. Finally, the furnace was slowly cooled down to room temperature at a speed of 10-30 °C/h.

X-ray diffraction (XRD) characterizations

Powder XRD investigation on polycrystalline LGT was carried out with a Bruker D8 advanced diffractometer equipped with Cu Kα radiation (λ = 1.54056 Å). The data were collected using a Ni-filtered Cu-target tube at room temperature in the 2θ range from 10 ° to 80 °. Single crystal XRD Diffraction Data were collected in the 2θ range from 2.01° to 27.44° using a Bruker APEX2 CCD area-detector diffractometer with graphite monochromated Mo Kα radiation (λ = 0.71073 Å) at 180 K. Because Li^+ is too light, in order to get high diffraction intensity of LGT lattice, the sample was cooled to low temperature of 180 K by liquid nitrogen to reduce the deleterious effect of lattice thermal vibration. A block-shaped LGT single crystal with dimensions of $0.10 \times 0.09 \times 0.08$ mm^3 was mounted on a glass fiber with epoxy. The structural model was refined using the SHELXL-97 routine (Sheldrick, 1997). Crystal data and refinement summaries are presented in Table 1 Final atomic coordinates and equivalent isotropic displacement parameters are listed in Table S1. Table S2 presents bond lengths (Å) and angles (deg.) for LGT.

Table 1 Crystal Data and Structure Refinement for LGT

Empirical formula	$LiGa_3Te_5$
Formula mass	854.10
Temperature	180 (2) K
Wavelength	0.71073 Å
Crystal system, space group	Trigonal, $R32$
Unit cell dimensions	$a=b$=14.343(7)Å; c=17.617(11)Å
Volume	3139(3) Å^3
Z, Calculated density	12, 5.422 Mg/m^3
Absorption coefficient	21.258 mm^{-1}
Crystal dimensions	0.10 ×0.09 ×0.08 mm^3
Theta range for data collection	2.01 to 27.44 deg.
Limiting indices	-18<=h<=18,-18<=k<=18,-22<=l<=22
Refinement method	Full-matrix least-squares on F^2
Final R indices [I>2sigma(I)]	$R1$ = 0.0170, $wR2$ = 0.0385
Extinction coefficient	0.000016(5)
Largest diff. peak and hole	1.452 and -0.566 e. Å^{-3}

High-resolution X-ray diffraction (HRXRD)

The quality of the grown LGT crystal was characterized using a Bruker D8 Advance X-ray diffractometer. We chose the rocking curve mode, with a generator setting of 30 kV and 35 mA.

Micro-hardness measurement

The micro-hardness of the grown LGT crystal was characterized with an HXS-1000A Vickers hardness tester fitted with a diamond indenter. The well-polished LGT crystal with smooth and dominant face was used for measurement. The hardness can be calculated using the formula Hv =18.18P/d^2, where P is the mass that is loaded onto the sample in kilograms and d is the average length of the diagonal indentation in millimetres.

Density measurement

The density of LGT at room temperature (20 ^{o}C) was measured by using the buoyancy method. Some deionized water in a beaker was weighed, and then a bulk LGT crystal hung by a filament was dipped into the water without touching the bottom or walls of the beaker. The net weight before and after immersion was then recorded.

Measurements of the thermal properties

The melting point of the LGT crystal was measured using a Mettler-Toledo TGA/DSC1/1600HT Thermal Analyzer in the range of 20-850 ^{o}C. About 60 mg of LGT was used for the DSC measurement. The LGT sample was placed in an Al_2O_3 crucible with Ar gas flowing at a rate of 60 ml/min to avoid oxidation of the LGT at high temperature. The heating rate was 10 ^{o}C/min. After the heating process was completed, the sample was

cooled down to room temperature at a rate of 10 ^{o}C/min. From the heating-cooling loop, the melting and crystallization points were obtained. The specific heat was measured between 30 ^{o}C and 300 ^{o}C at a heating rate of 10 ^{o}C/min. The thermal diffusion was measured by the laser flash method using a laser flash apparatus (NETZSCH LFA 447 Nanoflash) in the range from 28 to 210 ^{o}C. A (505)-faceted LGT wafer with a size of $4\times4\times1$ mm^3 was cut and roughly polished. The opposite surfaces are flat and paralleled, and both are coated with graphite for the measurements. When a laser pulse irradiates one side of the sample, the temperature rise on the opposite side is measured by an IR detector. The thermal diffusivity is then calculated using analytical software.

Optical transmission

The transmission spectra of LGT were recorded at room temperature using a Bruker Vertex 70 spectrometer. The silicon-diode detector works at room temperature over the visible and near-infrared range of 25000-8000 cm^{-1}. The liquid nitrogen-cooled mercury cadmium telluride (MCT) detector works over a mid-infrared spectral range of 12000-350 cm^{-1}, and the DTGS detector with works at room temperature over the far-infrared range of 700-10 cm^{-1}. A (505)-faceted LGT wafer with thickness of 2 mm was used for the measurements. The spectral range of our measurements covered 0.9-25 μm.

Results and discussion

Two-step synthesis and characterization of polycrystalline LGT

During the two-step synthesis of LGT, the following two chemical reactions take place.

$$2\ Ga + 3\ Te = Ga_2Te_3 \qquad (1)$$

$$2\ Li + 3\ Ga_2Te_3 + Te = 2\ LiGa_3Te_5 \qquad (2)$$
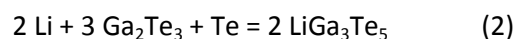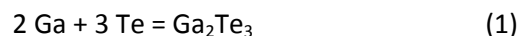
For the traditional single-temperature-zone method, the binary Li_2Te with high melting point is easily generated at first. The Li_2Te then encapsulates the molten Ga, which prevents further reaction between Ga and Te. As a result, it is difficult to obtain single-phase high-purity LGT using this method. A new method, two-step synthesis method, was used to synthesize LGT polycrystal. Firstly, a large amount of single-phase Ga_2Te_3 can be easily obtained, because the pressure inside the ampoule is not too high at the reaction temperature, and Ga and Te do not react with the quartz ampoule. The single-phase LGT can be then synthesized from Li, Ga_2Te_3, and Te by the second step reaction. A polycrystalline LGT ingot (shown in Fig. S1) was successfully synthesized. It was gray in color with many shiny reflective facets. The powder XRD characterization of polycrystalline LGT is presented in Fig. S2. The XRD pattern is in good agreement with the theoretical pattern calculated from single crystal data.

Modified vertical Bridgman growth of LGT single crystal

Fig. 2 shows the as-grown bulk LGT crystal (a) and a polished LGT plate (b). The as-grown LGT is gray in colour, 16 mm in diameter and 50 mm in length. A small (505)-faceted oriented LGT plate was cut and mechanically polished on two opposite sides for the measurements.
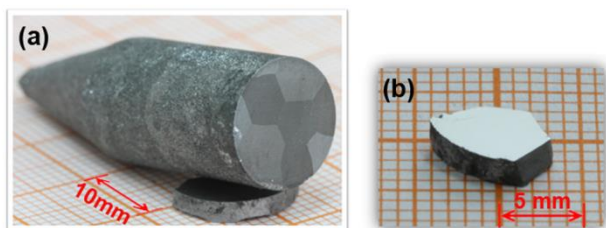
Fig. 2 (a) As-grown bulk LGT crystal with diameter of 16 mm and (b) (505)-faceted LGT plate polished on two sides.

Crystal structure

LGT crystallizes in a non-centrosymmetric space group, $R32$. The crystal cell parameters are $a = b = 14.343(7)$ Å; $c = 17.617$ Å, $Z = 12$, and $V = 3139$ Å^3, in accordance with Ref. 22. As shown in Fig 3(a) and (d), each Ga atom is coordinated to a tetrahedron of four Te atoms. As indicated in Table S2, the bond distances of Ga(1)-Te and Ga(2)-Te range from 2.580(2) to 2.662(3) Å and 2.609(1) to 2.653(3) Å, respectively. The Ga(1)Te$_4$ tetrahedra are connected along the c-axis in the form of prism structure (see Fig. 3(b)). The Ga(2)Te$_4$ tetrahedra extend in the a-b plane to form Ga(2)Te$_4$ layers, which are arranged in ABCABC order along the c-axis. In each layer, the Ga(2)Te$_4$ tetrahedra are linked by shared corners (see Fig. 3(e)). Therefore, the Ga(1)Te$_4$ tetrahedra chains parallel to the c-axis and the Ga(2)Te$_4$ tetrahedra layers perpendicular to the c-axis are connected to form the three-dimensional LGT structure (see Fig. 3(g)). The Li$^+$ cations are located in the cavities formed by the polyhedra. As is shown in Table S2, the bond distances for Li(1)-Te and Li(2)-Te range from 3.066 to 3.266 Å and 3.251 to 3.253Å, respectively. Both these values are larger than the theoritical value of 2.97 Å, which was calculated from the

normal Li$^+$ and Te^{2-} radii of 0.76 Å and 2.21 Å, respectively.[28, 30]

The HRXRD, density, and micro-hardness of LGT

A (505)-faceted LGT crystal plate with dimensions of $7 \times 5 \times 2$ mm^3, as shown in Fig. 2 (b), was cut and mechanically polished on two opposite sides for the HRXRD measurement. Fig. 4 shows the X-ray rocking curve of (505)-faceted LGT. The peak has good symmetry and the full width at half maximum (FWHM) is about 22.8 ´. However, the quality of as-grown bulk LGT can be improved by further growth optimizations or heat treatment after growth. The density of the LGT crystal at 20 $^{\circ}$C determined by the buoyancy method is 5.4(3) g cm^{-3}, which agrees well with the calculated value of 5.422 g cm^{-3} obtained from the crystallographic data (see Table 1). For micro-hardness study, the well-polished LGT crystal with smooth and dominant face was used. The loaded mass on the sample was 5 kg and the dwell period was 3 seconds. Under these conditions, the Vickers-hardness value of the LGT crystal is 313.7 kg/mm^2, which is equivalent to 3076.3 MPa. The result indicates that the mechanical strength of LGT is well suited for mechanical fabrication.

TG/DSC analysis

The TG/DSC heating-cooling loop of the LGT crystal is shown in Fig. 5. From the curves, it is seen that LGT is a congruent melting compound, which indicates that the crystal can be grown by the Bridgman method. The sharp endothermic peak at 787.84 ℃ and exothermic peak at 777.75℃ correspond to the melting and crystallization, respectively. Therefore, the supercooling temperature difference is 10.09 $^{\circ}$C, knowledge of which is very important for furnace design and for setting the crystal growth parameters. The LGT sample before and after DSC experiment was studied by XRD to test its thermal stability. As shown in Fig. 6, the XRD patterns of the LGT before and after DSC experiment are in good agreement with the calculated one. It indicates that LGT is thermally stable after heating and cooling between room temperature and 900 $^{\circ}$C.

Journal Name

RSCPublishing

ARTICLE
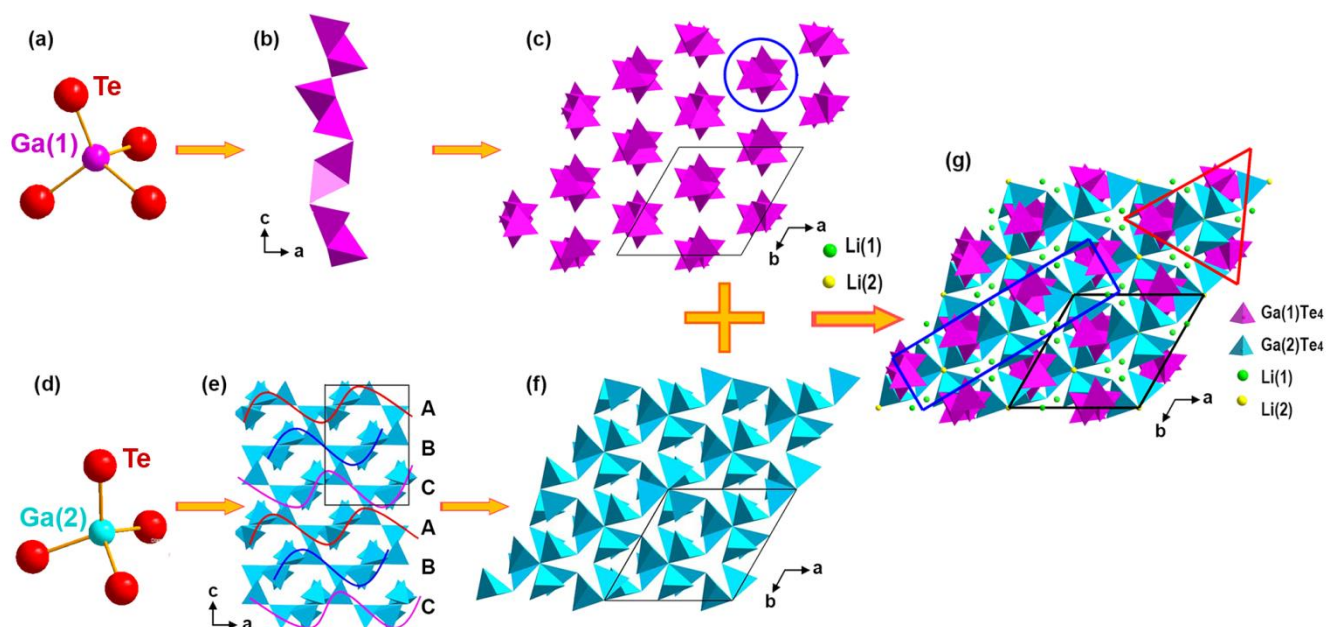
Figure 3. (a) and (d) are ball and stick representation of GaTe4; (b), (c) and (e), (f) are polyhedral representations of GaTe4 in 2D; (g) are polyhedral representation of the structure of LGT in 3D. Color codes: red spheres, O; pink spheres and polyhedra, Ga(1)Te4; light blue spheres and polyhedra, Ga(2)Te4; green spheres, Li(1); yellow spheres, Li(2).
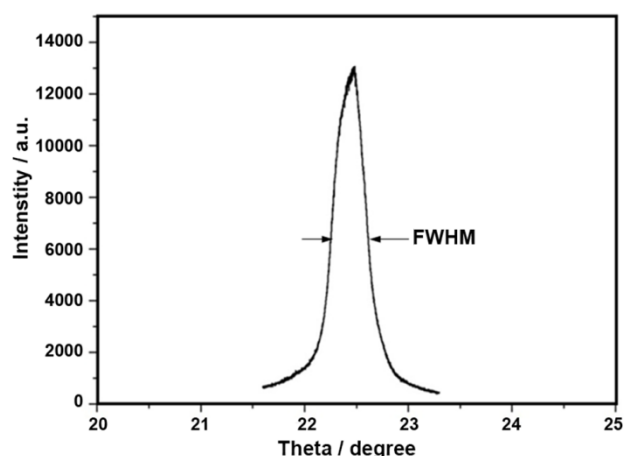
Fig. 4 Rocking curve of (505)-faceted LGT single crystal. Note that the FWHM is about 22.8′.
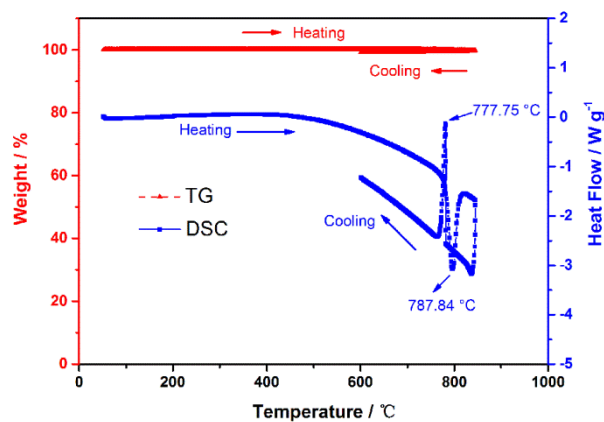
Fig. 5 TG/DSC loop of heating and cooling of LGT crystal. The peak temperatures of heating and cooling curves are indicated. Note that there are only one endothermic peak on the heating curve and one exothermic peak on the cooling curve of DSC and no obvious weight loss on the TG curve.
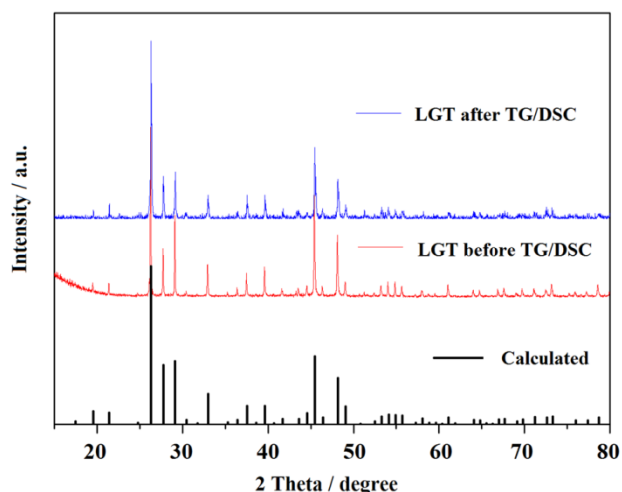
Fig. 6 XRD patterns of LGT samples before and after DSC experiment comparing with the calculated one.

Specific heat

The specific heat of LGT plotted as a function of temperature is shown in Fig. S3. The specific heat increases almost linearly from 0.24(2) $Jg^{-1}K^{-1}$ to 0.33(1) $Jg^{-1}K^{-1}$ as the temperature increases from 293 K to 573 K. It indicates that the crystal can tolerate more thermal energy at a high temperature, which is very important for high average power laser applications.

Thermal conductivity

The thermal conductivity κ can be calculated using the equation: $\kappa = \lambda \rho C_p$, where κ, λ, ρ, and C_p denote the principal thermal conductivity, thermal diffusion coefficient, density and specific heat, respectively. As shown in Fig. 7, the thermal diffusion of LGT was measured using the (505)-faceted plate. Therefore, the thermal conductivity perpendicular to the (505) face can be calculated. As is depicted in Fig. 7, the thermal conductivity of the crystal varies slightly from 0.587 to 0.618 $Wm^{-1}K^{-1}$, as the temperature increases from 25 to 210 °C.
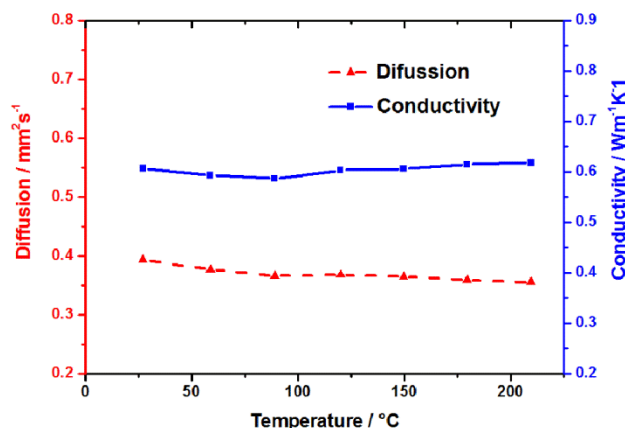
Fig. 7 Thermal diffusion and conductivity of LGT crystal.

Optical properties

Fig. 8 shows the room-temperature near-, mid-, and far-IR transmission spectra of the LGT crystal with incident light normal to the (505) plane. The sample for measurement is as-grown LGT crystal without any coating. The crystal exhibits good transparency from 3.5 to 18 μm at a level above 40%. For the ternary chalcogenide crystal LGT, the incongruent evaporation will give rise to the deviation from stoichiometry, which can produce some defects or inclusions. The sharp absorption peak near 11.3 μm is probably due to defects and inclusions in the crystal or multi-phonon absorption. The slightly rough fluctuations near 6-8 μm may be due to the surface quality of LGT sample or atmospheric absorption. The transmission of LGT can be improved by optimizing the crystal growth process or annealing in suitable atmosphere at a proper temperature, which is in progress. Further experiments will be carried out to investigate the intrinsic reasons for the absorption peak. Knowledge about any defects can help to optimize the parameters of the growth process and heat treatment. The transparency cut-off edges at short and long wavelength are at 0.9 and 25 μm, respectively. Even at 22 μm, the transmission level is about 20%. To the best of our knowledge, only a few crystals, such as GaSe, and GaP, are transparent above 15 μm. The chalcopyrite crystal $LiGaTe_2$ is phase-matchable for frequency doubling of CO_2 laser radiation at 10.6 μm possessing a very high figure of merit. However, its clear transparency range is only from 2.5 to 12 μm, and it is difficult to grow large crystal.[31, 32] As previously mentioned, for the important commercial MIR crystal ZGP, the serious two-photon and residual absorptions over 1-2 μm make it must be pumped by lasers with wavelength above 2 μm. Unfortunately, till now the crystal we grew is not large enough to cut the oriented LGT samples to measure the refractive index and NLO coefficients. The transparent range of LGT at level above 40% is from 3.5 to 18 μm. It is extremely hard for us to characterize the powder SHG efficient due to the laser sources limitation of our setup (1.064 μm and 2.1 μm). However, based on its non-centrosymmetric structure and wide MIR transparent wavelength range, we could predict that it should be a promising candidate for applications in mid- and far-IR and THz technology.
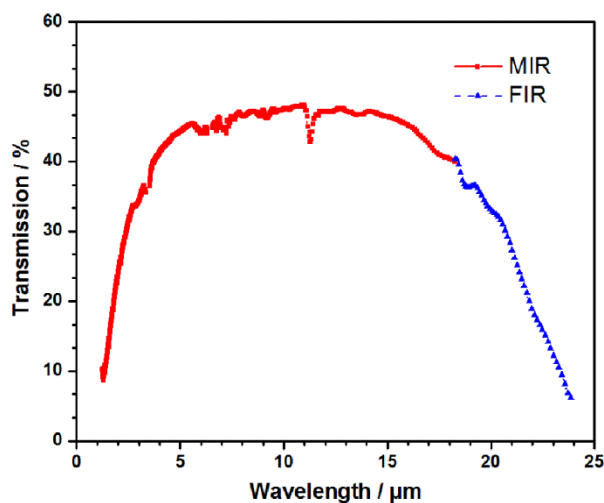
Fig. 8 Near-, mid-, and far-IR transmission spectra of the LGT crystal perpendicular to the (505) plane. Note that the sample is as-grown LGT without any coating.

Conclusions

We have successfully grown a large LGT single crystal with a diameter of 16 mm by a modified vertical Bridgman method. The detailed connections of the polyhedra in the LGT structure are presented. The Ga(1)Te4 tetrahedra chains parallel to the c-axis and the Ga(2)Te4 tetrahedra layers perpendicular to the c-axis are connected to form the three-dimensional LGT structure. The thermal properties of single crystal LGT were carefully studied by measuring the melting and crystallization points, specific heat, thermal diffusion and thermal conductivity. The room-temperature transmission of the crystal is higher than 40% from 3.5 to 18 μm, and the cut-off edges at short and long wavelength are 0.9 and 25 μm, respectively. The results indicate that LGT is a promising candidate for mid-infrared and THz technology. Further research on the optimization of crystal growth of LGT is in progress. We are trying to optimize the synthesis and growth process to get bulk LGT crystal with larger size and high quality. Then it is possible for us to fabricate the oriented LGT samples for measuring the refractive index and NLO coefficients, which is the aim of our future work.

Acknowledgements

Notes and references

[a] Address State Key Laboratory of Crystal Materials, Shandong University, Jinan, 250100, China.
[b] School of Chemistry and Engineering, Shandong University, Jinan, 250100, China.

*Corresponding Author, E-mail: txt@sdu.edu.cn

1. M. N. Islam, *Physics Today*, 1994, **47**, 34.
2. F. Tittel, D. Richter and A. Fried, in *Solid-State Mid-Infrared Laser Sources*, eds. I. Sorokina and K. Vodopyanov, Springer Berlin Heidelberg, 2003, pp. 458.
3. G. Edwards, R. Logan, M. Copeland, L. Reinisch, J. Davidson, B. Johnson, R. Maciunas, M. Mendenhall, R. Ossoff, J. Tribble, J. Werkhaven and D. O'Day, *Nature*, 1994, **371**, 416.
4. V. Petrov, *Opt. Mater.*, 2012, **34**, 536.
5. T. Sato, M. Mitsuhara and Y. Kondo, *Electron. Lett.*, 2007, **43**, 1143.
6. S. Sprengel, A. Andrejew, K. Vizbaras, T. Gruendl, K. Geiger, G. Boehm, C. Grasse and M.-C. Amann, *Appl. Phys. Lett.*, 2012, **100**.
7. K. Yang, H. Bromberger, H. Ruf, H. Schäfer, J. Neuhaus, T. Dekorsy, C. V.-B. Grimm, M. Helm, K. Biermann and H. Künzel, *Opt. Express*, 2010, **18**, 6537.
8. S. B. Mirov, V. V. Fedorov, K. Graham, I. S. Moskalev, I. T. Sorokina, E. Sorokin, V. Gapontsev, D. Gapontsev, V. V. Badikov and V. Panyutin, *IEE Optoelectronics*, 2003, **150**, 6.
9. I. T. Sorokina, E. Sorokin, S. Mirov, V. Fedorov, V. Badikov, V. Panyutin and K. I. Schaffers, *Opt. Lett.*, 2002, **27**, 1040.
10. A. A. Kaminskii, *Laser Photon. Rev.*, 2007, **1**, 93.
11. J. Faist, F. Capasso, C. Sirtori, D. L. Sivco, J. N. Baillargeon, A. L. Hutchinson, S. N. G. Chu and A. Y. Cho, *Appl. Phys. Lett.*, 1996, **68**, 3680.
12. J. Faist, F. Capasso, D. L. Sivco, C. Sirtori, A. L. Hutchinson and A. Y. Cho, *Science*, 1994, **264**, 553.
13. V. Badikov, D. Badikov, G. Shevyrdyaeva, A. Tyazhev, G. Marchev, V. Panyutin, V. Petrov and A. Kwasniewski, *Phys. Status Solidi RRL*, 2011, **5**, 31.
14. G. C. Bhar and R. C. Smith, *Phys. Status Solidi A*, 1972, **13**, 157.
15. Y. M. Andreev, V. V. Appolonov, Y. A. Shakir, G. A. Verozubova and A. I. Gribenyukov, *J. Korean Phys. Soc.*, 1998, **33**, 320.
16. G. C. Bhar and P. Kumbhakar, *J. Appl. Phys.*, 2000, **87**, 4638.
17. D. W. Fischer, M. C. Ohmer, P. G. Schunemann and T. M. Pollak, *J. Appl. Phys.*, 1995, **77**, 5942.
18. D. W. Fischer and M. C. Ohmer, *J. Appl. Phys.*, 1997, **81**, 425.
19. A. F. Nieuwenhuis, C. J. Lee, P. J. M. van der Slot, I. D. Lindsay, P. Groß and K. J. Boller, *Opt. Lett.*, 2008, **33**, 52.
20. S. C. Kumar, M. Jelínek, M. Baudisch, K. T. Zawilski, P. G. Schunemann, V. Kubeek, J. Biegert and M. Ebrahim-Zadeh, *Opt. Express*, 2012, **20**, 15703.
21. P. Kumbhakar, T. Kobayashi and G. C. Bhar, *Appl. Optics.*, 2004, **43**, 3324.
22. K. L. Vodopyanov, J. P. Maffetone, I. Zwieback and W. Ruderman, *Appl. Phys. Lett.*, 1999, **75**, 1204.
23. T.-J. Wang, Z.-H. Kang, H.-Z. Zhang, Q.-Y. He, Y. Qu, Z.-S. Feng, Y. Jiang, J.-Y. Gao, Y. M. Andreev and G. V. Lanskii, *Opt. Express*, 2006, **14**, 13001.
24. L. Isaenko, I. Vasilyeva, A. Merkulov, A. Yelisseyev and S. Lobanov, *J. Cryst. Growth*, 2005, **275**, 217.
25. L. I. Isaenko and I. G. Vasilyeva, *J. Cryst. Growth*, 2008, **310**, 1954.
26. T. Kamijoh and K. Kuriyama, *J. Appl. Phys.*, 1981, **52**, 1102.
27. L. Kienle and H. Deiseroth, *Z. Krist-new. Cryst. St*, 1998, **213**, 1.
28. H. J. Deiseroth, L. Kienle, H. Günther and M. Hartung, *Z. Anorg. Allg. Chem.*, 2000, **626**, 302.
29. T. Xutang, W. Shanpeng, L. Guandong and J. Minhua, ed. S. University, China, 2011.
30. R. Shannon, *Acta Crystallogr. A*, 1976, **32**, 751.

31. L. Isaenko, P. Krinitsin, V. Vedenyapin, A. Yelisseyev, A. Merkulov, J. J. Zondy and V. Petrov, *Cryst. Growth Des.*, 2005, **5**, 1325.
32. V. Petrov, L. Isaenko, A. Yelisseyev, P. Krinitsin, V. Vedenyapin, A. Merkulov and J. J. Zondy, *Journal of Non-Crystalline Solids*, 2006, **352**, 2434.